Seasonal and inter-annual variability in ^{13}C composition of ecosystem carbon fluxes in the U.S. Southern Great Plains

Margaret S. Torn*
Corresponding author. Lawrence Berkeley National Laboratory and UC Berkeley
One Cyclotron Rd, 90R111, Berkeley, CA, 94720, USA
mstorn@lbl.gov

Sebastien Biraud
Lawrence Berkeley National Laboratory, Earth Sciences Division, USA

Chris J. Still
University of California, Santa Barbara, Geography Department, USA

William J. Riley
Lawrence Berkeley National Laboratory, Earth Sciences Division, USA

Joe A. Berry
Carnegie Institution of Washington, Department of Global Ecology, USA

September 22, 2010

Keywords/phrases:
Stable isotopes ($^{13}CO_2$)
C_3 and C_4 vegetation types
Carbon fluxes and inverse models
Isofluxes
Grasslands and agriculture

* Corresponding author
Email: mstorn@lbl.gov

Abstract

The $\delta^{13}C$ signature of terrestrial carbon fluxes (δ_{bio}) provides an important constraint for inverse models of CO_2 sources and sinks, insight into vegetation physiology, C_3 and C_4 vegetation productivity, and ecosystem carbon residence times. From 2002-2009, we measured atmospheric CO_2 concentration and $\delta^{13}C$-CO_2 at four heights (2 to 60 m) in the U.S. Southern Great Plains (SGP) and computed δ_{bio} weekly. This region has a fine-scale mix of crops (primarily C_3 winter wheat) and C_4 pasture grasses. δ_{bio} had a large and consistent seasonal cycle of 6–8‰. Ensemble monthly mean δ_{bio} ranged from -25.8±0.4‰ (±SE) in March to -20.1±0.4‰ in July. Thus, C_3 vegetation contributed about 80% of ecosystem fluxes in winter-spring and 50% in summer-fall. In contrast, prairie-soil $\delta^{13}C$ values were about -15‰, indicating that historically the region was dominated by C_4 vegetation and had more positive δ_{bio} values. Based on a land-surface model, isofluxes ($\delta_{bio} \times$ NEE) in this region have large seasonal amplitude because δ_{bio} and net ecosystem exchange (NEE) covary. Interannual variability in isoflux was driven by variability in NEE. The large seasonal amplitude in δ_{bio} and isoflux imply that carbon inverse analyses require accurate estimates of land cover and temporally resolved $^{13}CO_2$ and CO_2 fluxes.

1 Introduction

Atmospheric $\delta^{13}C$-CO_2 values (δ_{atm}) provide insight into ecosystem carbon fluxes and the plant physiological processes that drive them. For example, δ_{atm} is used by inverse and forward models to quantify oceanic, terrestrial, and fossil carbon sources and sinks (Ciais et al. 1995; Fung et al. 1997; Rayner et al. 1999, 2008). Because air-sea gas exchanges do not strongly affect δ_{atm} whereas terrestrial CO_2 exchanges do, δ_{atm} has been used to distinguish land versus ocean carbon fluxes (Keeling et al. 1989; Tans et al. 1993; Enting et al. 1995; Francey et al. 1995; Battle et al. 2000) and to attribute interannual variability in the global carbon sinks (Keeling et al. 1995; Francey et al. 1995; Langenfelds et al. 2002; Le Quéré et al. 2003; Randerson et al. 2002). These applications require prior information about the magnitude and isotopic signature of the ecosystem carbon exchanges (δ_{bio}; Bakwin et al. 1998) that force these atmospheric changes. Likewise, coal, petroleum products, and natural gas have different $\delta^{13}C$ signatures, nearly all distinct from terrestrial ecosystem exchange. Finally, δ_{atm} and δ_{bio} are also useful for predicting biosphere responses to CO_2 fertilization (e.g., Randerson et al. 1999).

The $\delta^{13}C$ signature of land surface–atmospheric carbon exchange (photosynthetic uptake and respiration) is also useful for distinguishing the proportional contribution to total flux by plants using different photosynthetic pathways: C_4 plants discriminate less than C_3 plants against $^{13}CO_2$ during photosynthesis, as described below. Being able to distinguish C_3 and C_4 exchange is useful for studying C_3 and C_4 plant phenology, their different responses to changes in CO_2 and climate, and their competitive coexistence (Niu et al. 2008), as well as the ability to correctly simulate these in carbon cycle models is critical to the de-convolution problem.

Currently, the application of isotopic tracers at ecosystem and global scales is limited by insufficient measurements of $^{13}CO_2$ fluxes (isofluxes) and limited confidence in models that predict them. In fact, a number of studies have concluded that the largest uncertainties associated with land:ocean partitioning are in modeling spatial and temporal variations in terrestrial ^{13}C fractionation and isotopic disequilibria between gross primary productivity and respiration (Heimann and Meier-Raimer 1996; Rayner et al. 1999, 2008; Townsend et al. 2002; Randerson et al. 2005; Scholze et al. 2008). Global inversion models are very sensitive to the magnitude and isotopic signature of photosynthesis and respiration. For example, a 3‰ difference in

photosynthetic discrimination globally can yield a 0.7 Pg y^{-1} difference in the estimated terrestrial carbon sink and a 0.2‰ underestimate in the GPP-ecosystem respiration disequilibrium can yield about a 0.5 Pg y^{-1} difference (Ciais et al. 1995, 1999; Fung et al. 1997).

One of the largest effects on land-surface isotopic fluxes is the difference between C_3 and C_4 plant types. Because of biochemical and anatomical differences, C_3 and C_4 plants fractionate against $^{13}CO_2$ to different degrees during photosynthesis (Farquhar et al. 1989). Typically, C_4 and C_3 photosynthetic assimilation have isotope fractionation of 4 and 20‰, respectively, and tissue of these plant types has $\delta^{13}C$ values of roughly -12‰ and -28‰. As a result, changes in land cover, such as conversion of tropical forests to pastures or sugar cane, can have large effects on δ_{atm} and therefore its interpretation in atmospheric carbon budgets (Ciais et al. 1999; Townsend et al. 2002; Still et al. 2003b). Considering the isotopic disequilibria caused by land use changes to C_4 pastures and crops or interannual C_3/C_4 variations driven by climate, Scholze et al. (2008) concluded that not accounting for C_4 disequilibria in a ^{13}C deconvolution calculation can alter the land:ocean partitioning by 1 Pg C yr^{-1}. Better understanding of spatial and temporal variations in ecosystem C_3/C_4 fractions is therefore critical to accurately assess variation in terrestrial ^{13}C fractionation as well as the resulting isotope disequilibria for 3-D inversion studies employing both CO_2 and $^{13}CO_2$ (Still et al. 2003b).

Grasslands with a mixture of C_3 and C_4 species are found in temperate North America, South America, Asia, and Australia (Collatz et al. 1998). Historically, the dominant vegetation cover of the U.S. Great Plains was shortgrass and tallgrass prairie that contained a mixture of C_4 grasses and C_3 grasses and forbs, and riparian forests (McNab and Avers 1994). Much of the native prairie has been converted to cropland, grazed grasslands, and pastures, with the latter two subject to fairly frequent burning (Knapp et al. 1998). In mixed grasslands, C_3 grasses generally grow in spring and early summer, while C_4 grasses dominate during mid- and late summer (Kemp and Williams 1980; Freeman 1998; Knapp et al. 1998). This seasonal partitioning results from differences in the biochemistry of each photosynthetic pathway (Ehleringer et al. 1997; Collatz et al. 1998) and their largely temperate (C_3) and tropical (C_4) origins (Edwards and Still 2008). The C_4 fraction of prairie grasses increases from the northwest to the southeast of the Southern Great Plains, similar to the trend across the Great Plains as a whole (Epstein et al. 1997; Tieszen et al. 1997; Knapp et al. 1998).

The Southern Great Plains is an excellent location for studying the $\delta^{13}C$ value of terrestrial carbon fluxes (δ_{bio}) because there is comprehensive meteorological and carbon cycle infrastructure, simple topography, and fairly consistent wind direction. Furthermore, land cover is similar to other temperate mixed agricultural and C_3/C_4 grasslands and the region is located in the domain of many forward and inverse model studies of CO_2 sources and sinks.

The objectives of this study were to characterize the $\delta^{13}C$ values of ecosystem respiration and net ecosystem exchange from a multi-field area of the SGP over eight years and use this record to investigate the (1) seasonal and interannual variation in ^{13}C signature of these fluxes; (2) relative contribution of C_3 versus C_4 productivity to CO_2 fluxes observed at a centrally-located 60 m tower; and (3) seasonal and interannual variation in sub-regional ^{13}C isofluxes. We generated weekly estimates of δ_{bio} at the SGP 60 m tower for 8 years, by collecting 16 flasks per week from four tower heights and calculating the $\delta^{13}C$ value of nighttime respiratory and daytime net ecosystem (NEE) carbon fluxes using the Keeling plot approach (Keeling 1959 and 1961). To estimate isofluxes, we combined output from a spatially explicit, isotope-enabled ecosystem model (ISOLSM; Riley et al. 2002, 2009; Aranibar et al. 2006) with a simple footprint estimation.

2 Methods

2.1 Site Description

Our study region is the U.S. Southern Great Plains (SGP), centered in north-central Oklahoma (Figure 1) and extending to southern Kansas. The climate is continental to semi-arid (Figure 2). Mean annual precipitation in the region ranges from 1270 mm in the southeast to 380 mm in the NW. Oklahoma state mean annual temperature is about 15ºC, but mean daily temperatures frequently exceed 20 ºC during summer months. There is strong horizontal advection, predominantly from the south except during some spring periods (Figure 3).

Land cover in SGP is dominated by pasture, grazing lands, and annual crops, with winter wheat covering more than 40% of cropland (Figure 1). Other crops, such as sorghum (C_4), soybean (C_3), oats (C_3), barley (C_3), and corn (C_4) are commonly grown in summer. The typical field size is a quarter section, or 64.7 ha. Because land holdings are small and the crops are annuals, land cover has fine scale spatial heterogeneity and individual fields can change cover type from year to year.

The U.S. Department of Energy Atmospheric Radiation Management Program (ARM) Climate Research Facility (ACRF) supports a large testbed, roughly 300×300 km, for measurements and modeling in the Southern Great Plains (Ackerman et al. 2004). All atmospheric and climatic variables measured in the ACRF are available from the ARM Data Archives (www.archive.arm.gov). The Oklahoma and Kansas Mesonet networks of meteorological stations also contribute data to our analysis. The main site for our measurements is the ACRF Central Facility (36.61°N, 97.49°W), located in the center of the testbed in the midst of farmland in Lamont, Oklahoma.

2.2 Atmospheric gas sampling for CO_2 and $^{13}CO_2$

Atmospheric samples were collected from a 60 m tower at the Central Facility. Instruments and flask samplers were installed in a climate-controlled shed at the base of the tower. Air was pulled from inlets mounted on the tower at 2, 4, 25, and 60 m through 3/8" Dekaron tubing to the shed. The stainless steel inlet assemblies contain a quartz filter and fine metal frit. In the shed, air was dried by passage through a condensing unit and collected in glass flasks.

We used an automated system for trapping the air into glass flasks. Sampling tubes from each of the four heights on the tower led to a 4-port manifold with automated valves. A datalogger controlled which sampling height was routed to the flask box. Incoming sample air was pumped at more than 500 ml min^{-1} through a multi-port valve (Valco ST configuration E 16 position valve) to 100 ml glass flasks (Kontes Custom Glass Shop). Before sampling, the flasks were filled with dry air from a cylinder, closed, and shipped to the Central Facility. On the collection day, flasks were placed in the 16-flask unit and opened. They were sealed from outside air by the multi-port valve. To collect a sample, the valve position changed to allow air from the tower inlet to flow through the flask. After 3 minutes, the automated valve changed position, sealing the flasks. At the end of the diel cycle, the flask-valves were closed manually and the flasks were shipped to California for analysis.

Flask samples were analyzed at the Carnegie Institution of Washington (Stanford, California) with an integrated system that measures the CO_2 concentration and isotope ratios ($\delta^{13}C$ and $\delta^{18}O$) of small air samples, as described by Ribas-Carbo et al. (2002). Five repeated measurements on the air in each flask yields high-precision data, with standard errors of the

measurement around 0.5 ppm for CO_2 and 0.03‰ for $\delta^{13}C$ for each data point. Gases from NOAA-ESRL are used for calibration and span of the instrument. All values are reported using the delta (δ) notation with per mil (‰) variations relative to VPDB (Vienna Pee Dee Belemnite):

$$\delta^{13}C\ (‰) = \left[\frac{(^{13}C/^{12}C)_{sample}}{(^{13}C/^{12}C)_{VPDB}} - 1\right] \times 1000‰ .$$

2.3 Flask sampling protocol

To estimate δ_{bio}, we collected 16 flask samples over 1–2 days every week, with the heights and timing of sampling following either a "nighttime" or "diel" protocol. We alternated protocols. Every other week, we collected a flask sample at each of the four heights (2, 4, 25, 60 m) at each of four time points in the dark (22:00, 00:00, 2:00, and 4:00 local time). This is referred to as the "nighttime" protocol. On the alternating weeks, we collected a flask sample at two heights (2, 60 m) at each of 8 time points, starting in the late afternoon and continuing to mid-afternoon of the next day (18:00, 21:00, 00:00, 3:00, 6:00, 9:00, 12:00, and 15:00 local time). This is referred to as the "diel" protocol. We split the data from the diel collection, using sunrise and sunset as boundaries, to look at carbon exchange when it was dark (21:00-6:00) and light (9:00-15:00); the 18:00 flasks were used for the diel-dark keeling plots when sunset occurred before 18:00 local time (for a total of 8-10 flasks for dark and 6-8 for daylight). These δ_{bio} values are referred to as diel-dark and diel-light, respectively.

2.4 NOAA flasks

We collected two flasks at 60 m at roughly 2 pm local time each week on the day that the Keeling plot collection began. The samples were collected using a flask package built by NOAA and the samples were analyzed by NOAA-ESRL. These data are used in the ESRL GLOBALVIEW product and were used in this study to provide validation for the atmospheric δ_{atm} data used in the Keeling plot mixing model. We also collected flasks in the free troposphere by aircraft each week that were analyzed by NOAA.

2.5 Keeling plot analysis

To estimate the ^{13}C isotopic signature of ecosystem CO_2 exchange, some studies have used the mass-weighted-average plant biomass ^{13}C as a proxy, but it is preferable to measure the isotopic signature of the CO_2 flux directly because this gives the flux-weighted physiological

activity of C_3 and C_4 plants rather than simply their relative biomass abundance (e.g., Tieszen et al. 1997; Dawson et al. 2002). One established method for estimating δ_{bio} is a mixing model called the 'Keeling plot', based on measurements of atmospheric CO_2 mixing ratios and ^{13}C values (see Methods; Keeling 1959 and 1961).

We estimated δ_{bio} as the intercept of a 'Keeling plot' in which $\delta^{13}C$ values were regressed against the reciprocal of CO_2 concentration (i.e., $[CO_2]^{-1}$) for a series of flask measurements (Keeling 1958, 1961; Flanagan and Ehleringer 1998; Yakir and Sternberg 2000; Pataki et al. 2003); see Figure S1 in online supporting information.

We used a linear regression model (type I) to calculate intercept values. Some studies have advocated a model II, or geometric mean, regression to incorporate errors in both the concentration and isotope values (Friedli et al. 1987; Flanagan et al. 1996; Zar 1996; Sokal and Rohlf 1995; Bowling et al. 1999; Harwood et al. 1999; Pataki et al. 2003). It has been shown, however, that there is almost no difference between these two regression models at high correlation coefficient values such as those in the Keeling plots reported in this study (Zobitz et al. 2006) and it is more straightforward to estimate errors with a type I model (Sokal and Rohlf 1995; Laws 1997; Zar 1996).

We applied quality standards to our regression intercept values by using only those collections for which the intercept standard error (SE) for the regression of $\delta^{13}C$ on $1/CO_2$ was less than 1.5‰. We evaluated the potential bias introduced by using standard error (SE), R (correlation coefficient), and CO_2 mixing ratio ranges as cutoff criteria and found no discernable bias in intercept values created by the SE cutoff. Keeling plots were analyzed with fewer than 16 flasks if some flasks did not pass laboratory analytical checks.

2.6 Fractional contribution of C_3 and C_4 plant types to ecosystem carbon exchange

To calculate the fractional contribution of C_3 and C_4 plants to ecosystem carbon exchanges (f_{C3} and f_{C4}, respectively), we used a two-member mixing model based on the assumption that NEE variations in these plant types drives the observed variations in δ_{bio} as: $\delta_{bio} = \delta_{C3} f_{C3} + \delta_{C4} f_{C4}$, where δ is the $\delta^{13}C$ value, and subscripts indicate the measured Keeling plot result (δ_{bio}) or the C_3 and C_4 contributions. As a two member mixing model, we set $f_{C3} + f_{C4} = 1$. Substituting $f_{C3} = 1 - f_{C4}$ and rearranging gives: $f_{C4} = \frac{(\delta_{bio} - \delta_{C3})}{(\delta_{C4} - \delta_{C3})}$.

Given measurements of CO_2 and δ_{atm} in the nocturnal boundary layer and ^{13}C end members for C_3 and C_4 plant types, Keeling plot analysis has been used to infer the C_4 respiration fraction at ecosystem to regional scales (Miranda et al. 1997; Still et al. 2003a; Lai et al. 2003;). The partitioning relies on the large and fairly consistent $\delta^{13}C$ offset between C_3 and C_4 plants. The offset can be affected by variable C_3 isotope fractionation resulting from moisture stress, with much less variation in C_4 grass isotopic composition (Farquhar et al. 1989; Henderson et al. 1992; Mole et al. 1994; Buchmann et al. 1996; Still et al. 2003a).

2.7 Isotopic end members for C_3 and C_4 plant types

We estimated the isotopic end members for each plant type from leaf $\delta^{13}C$ values published by Still et al. (2003a) and of leaf samples that we collected. These are a proxy for average $\delta^{13}C$ values of leaf photosynthetic uptake and whole plant respiration. More accurate estimates would be generated by direct measurements of these fluxes, for C_3 and C_4 plant types, over the region, for each time point. We lack such measurements but note that they would do little to advance our main goal which is to define the influence of this region on the atmosphere and to test our ability to simulate this forcing.

We collected leaf and soil samples in fields within 10 km of the Central Facility as well as at the U.S. Department of Agriculture Agricultural Research Service Grazinglands Research Laboratory (GRL) near El Reno, Oklahoma (35° 33'N, 98° 02'W). At GRL, vegetation was sampled in ten 50×50 cm quadrats per field, and sorted into C_3 functional groups (forbes, sedges, and annual cold season grasses) and one C_4 functional group (perennial warm season grasses). Green leaves from each functional group were analyzed for $\delta^{13}C$. Vegetation values reported here are the average of samples collected once a month for five months between May and December in 2005 and 2006. Near the Central Facility, green leaves were sampled in wheat fields monthly January-May, 2003. For a prairie near the Central Facility, Still et al. (2003b) sampled 16 plant species through the 1999 growing season.

Soils were sampled to 1 m depth in two fields of lightly grazed prairie at GRL, using a Giddings brand hydraulic corer (n=10 per field; 7 depths per core). One field was subject to a controlled burn in March 2005 and the other had not been burned for more than 10 years. Collection dates were March 2005 (right after the burn) and March 2007. The soil core was split

length-wise. One half was sieved at 2 mm and roots were removed by hand picking for five minutes. The sieved soil was dried at 50ºC and ground to produce a homogenized bulk sample.

Organic carbon content and $\delta^{13}C$ were determined on soil and leaf samples with an elemental analyzer connected to an isotope ratio mass spectrometer at the University of California, Berkeley Center for Stable Isotope Biogeochemistry and the Northern Arizona University Colorado Plateau Stable Isotope Laboratory.

The $\delta^{13}C$ values for leaves and soil carbon at GRL, Central Facility, and Still et al. sites are given in Table 1. The consistency in leaf $\delta^{13}C$ values across months, years, and fields suggests these are representative average C_3 and C_4 leaf values for this region.

2.8 Isoflux

Isoflux (I, μmol m^{-2} s^{-1} ‰) is defined as the CO_2 flux multiplied by its $\delta^{13}C$ value (Bowling et al. 2008; Riley et al. 2003). As a result of the sign convention for fluxes, in which negative flux is a transfer of carbon from atmosphere to ecosystem, a positive isoflux implies transfer of ^{13}C-depleted CO_2 from the atmosphere, thereby enriching δ_{atm}.

We estimated weekly average NEE and ecosystem respiration with a spatially-explicit, isotope-enabled land-surface model (ISOLSM; Riley et al. 2009) that has been calibrated and tested in this region against eddy flux tower observations (Billesbach et al. 2004; Fischer et al. 2008) and is driven by Mesonet and ARM Extended Facilities climate observations and MODIS-derived land cover and LAI. For the simulations used here, we have imposed a time varying C_3/C_4 fraction based on the work by Still et al. (2003a); we note that the partitioning in that work is consistent with that calculated in the current study. Using methods described in Aranibar et al. (2006) and based on those described by Farquhar et al. (1989), ISOLSM predicts photosynthetic discrimination and respiratory ^{13}C fluxes as a function of plant type, phenology, water status, and atmospheric conditions.

The predicted NEE and δ_{bio} used here are weekly average values in the upwind direction of the tower. We did not estimate a proper footprint for the Keeling plot intercept. Rather, we used the land surface of SGP in the weekly-average wind direction (denoted here as α). If α was more than 5° E or W of South, we used the land surface of the SW or SE quadrant of SGP, respectively. If α was less than 5º off south, we used the southern half of SGP as the source area.

NEE and δ_{bio} were modeled at 10 km resolution in the selected area. The use of weekly average NEE implicitly treats the weekly $\delta^{13}C$ value of photosynthetic uptake and respiration as the same. This appears to be a reasonable simplification for SGP, since the difference between δ_{bio} for light and dark periods was small, especially compared to the seasonal signal (see Results section). We predicted isoflux by multiplying ISOLSM predictions of δ_{bio} and NEE.

3 Results

3.1 Atmospheric CO_2 and $^{13}CO_2$

Atmospheric CO_2 mixing ratio and δ_{atm} in the Southern Great Plains display a distinct seasonal cycle and interannual trend from 2002–2009 (Figure 4). For both species, the free troposphere (airborne sampling) values at SGP tracked the global background values for 36º N very closely (Figure 4). Within the planetary boundary layer, there was considerable diurnal variability in CO_2 concentrations. Considering only those data collected in the afternoon, when the boundary layer was well mixed (dark blue symbols in Figure 4), the timing of seasonal peaks and troughs is similar to that in the free troposphere but the amplitude is greater, reflecting the continental influences of land fluxes and atmosphere dynamics. At night, CO_2 accumulates in the lower atmosphere, as there is no photosynthetic uptake and only ecosystem respiratory fluxes.

δ_{atm} values also have a large diurnal range because δ_{bio} of respired CO_2 is much more negative than the δ value of the background atmosphere. The stable nocturnal boundary layer acts somewhat like a chamber and the buildup of CO_2 changes δ_{atm} on a given night by as much as 3‰. Including day and nighttime data, the range in CO_2 concentration within any year was 75 ppm and in δ_{atm} was more than 3.5‰ (Figure 4).

3.2 $\delta^{13}C$ values of ecosystem carbon exchanges (δ_{bio})

We used the diurnal cycle in CO_2 and δ_{atm} and the boundary layer's chamber-like effect to analyze the flasks collected between 2 and 60 m with a Keeling plot regression analysis (Figure S1). The flask-collection protocols sampled a vertical and temporal CO_2 gradient created by ecosystem respiration into a stable nocturnal boundary layer ("nighttime" and "diel-dark" protocols) or by net photosynthetic drawdown during the day ("diel-light" protocol) (Figure 5, Figure S2)

Between January 2002 and December 2009, we collected a set of flasks almost every week (5,791 analyses) and generated 340 Keeling plots that are fairly evenly spaced in time over the eight-year period (Figure 6). Of those, 109 Keeling plots had SE > 1.5‰ (including all Keeling plots with a CO_2 span below 5 ppm) and were excluded from this analysis, leaving 231 weekly δ_{bio} signatures in the time series reported here. A comparison among SE, R-values, and CO_2 range of all Keeling plots is presented in Figure S2. Large temporal and vertical $^{13}CO_2$ gradients and high isotope-measurement precision yielded high regression coefficients and low SE for flask sets with CO_2 ranges as low as 5–10 ppm.

We computed separate Keeling plot intercepts for the light and dark periods of the diel sampling. There was no difference between the diel-dark δ_{bio} and the full diel value (Figure 5a) for all weeks when both intercepts were significant. We conclude that the nighttime respiration observations dominate the diurnal Keeling plot.

There were 33 weeks with diel-light intercepts with SE < 1.5‰, distributed across spring, summer, and fall, and in every year. Although it is more difficult to obtain significant Keeling plots in the day time, 14 weeks had SE < 0.5‰ and 26 had SE < 1‰.

There were 30 weeks for which both diel-light and diel-dark intercepts had SE<1.5‰, allowing us to compare periods influenced by photosynthetic uptake and respiration versus just respiration (Figure 5b). Of these, 16 weeks showed no significant difference between light and dark Keeling plot intercepts, with a mean difference of only 0.03‰. (The mean of the absolute value of the differences was 0.77 ± 0.15‰.) Considering all 30 pairs, the diel-dark values were slightly more negative than the diel-light values (mean dark–light difference -0.49 ±0.27‰ and mean of absolute differences 1.27±0.16‰). There was no seasonal pattern to the dark–light differences. Unless noted, subsequent results refer to respiration δ_{bio}, calculated from the nighttime (n=97 weeks) and diel-dark (n= 116 weeks) protocols.

Weekly respiration δ_{bio} measured at the tower ranged between -16‰ (summer) to -32‰ (winter), with only 3 values were below -30‰. There was a consistent seasonal cycle, with a minimum in winter and a maximum in summer and a seasonal amplitude of about 8‰ (Figure 6). The ensemble monthly means (n=5–8 months) ranged from a high of -20.1±0.4‰ (±SE) in July to a minimum of -25.8±0.4‰ in March (Table 2). There was no apparent secular annual trend in the peak, minimum, or timing of the seasonal cycles (Figure 6). The values generated by

the nighttime and diel-dark protocols, although slightly different, had the same seasonal patterns and magnitudes (Figure 6; see Figure S3 for a plot of nighttime vs. diel δ_{bio}).

To look for anomalies in weekly δ_{bio}, we computed the difference between monthly average Keeling plot values for each month and the ensemble mean for that month (Table 2), and compared these to means and anomalies in monthly average precipitation, temperature, and vapor pressure deficit. The study period had significant inter-annual variability in monthly rainfall but overall was slightly drier than the climatological average (Figure 2). 2006 had very low rainfall in the winter, summer, and fall. The following year had the wettest June in the Oklahoma written record. Although SGP specific humidity peaks in summer , high temperatures resulted in maximum vapor pressure deficit in summer. During the period of study, vapor pressure deficit was highest in summer 2006 and July 2003 (Figure 2).

In 2006, the dry spring resulted in widespread failure of the winter wheat crop, corresponding to less C_3 NEE and thus anomalously positive spring δ_{bio} values (Figure 6). For the whole 8-year period (n = 88 monthly averages; Table 2), we found no correlation between monthly precipitation anomalies and δ_{bio} anomalies, but considering the summer months only (July, August, September) there was a positive correlation with a small but significant slope. Specifically, higher rainfall in summer months was correlated with more positive δ_{bio} values. For July and September, precipitation anomalies explained >70% of the variance in monthly δ_{bio} anomalies, with a slope of 0.03‰ per mm additional rain ($p < 0.04$; n = 6 for each month except 2004 and 2009). Precipitation anomalies in July and September ranged from +40 mm to -63 mm, associated, according to this slope, with anomalies in the mean monthly δ_{bio} of +1.2‰ and –1.9‰, respectively. (The regression for August months was not significant and had a different slope, resulting in a summer (July-August-September) regression with $R^2 = 0.2$, slope = 0.01 ‰ mm^{-1} $p < 0.08$; n = 19.)

3.3 Fractional contribution of C_3 and C_4 plant types to ecosystem carbon exchange

δ_{bio} can be used to estimate the relative contribution of C_3 versus C_4 fluxes in the measurement footprint (Still et al. 2003a; Lai et al. 2003). Using the two-member mixing model and leaf-tissue end members given in the Methods and Table 1, we estimated that ecosystem carbon exchange was 85% C_3 in March to 50% C_3 in summer (Table 2; Figure S4). The fraction of total ecosystem exchange ascribed to C_3 plants peaked in winter because there was almost no

C_4 uptake or respiration. In absolute terms, C_3 uptake fluxes peaked in April and May, according to eddy flux data and land cover maps (Billesbach et al. 2004; Fischer et al. 2008; Riley et al. 2009). Note that the influence of ecosystem fluxes on atmospheric $\delta^{13}C$ depends both on the isotopic ratio and magnitude of NEE.

The uncertainty in C_4/C_3 ratio due to uncertainty in the intercept, propagated as in Phillips and Gregg (2001), was less than two percentage points. For end members, the variation in leaf $\delta^{13}C$ values, among species, sites, seasons, and years that we sampled, was less than 0.2‰. A sensitivity analysis using this range of uncertainty in end members gives an uncertainty in f_{C3} and f_{C4} of 1.4%. Thus, the uncertainty in using leaf tissues to represent leaf fluxes (Bowling et al. 2008; Cernusak et al. 2009) is much smaller than the magnitude of temporal patterns observed.

3.4 Isofluxes

To investigate the influence of our observed patterns in δ_{bio} on the atmosphere, we used ISOLSM to predict ecosystem carbon exchange and calculate isofluxes for 2006–2008. The NEE predicted for the SGP area upwind of the tower is shown in Figure 7a. ISOLSM predicted net CO_2 uptake (regional average uptake > 2 μmol C m^{-2} s^{-1}) from March to October. The variability in NEE reflects mainly seasonal phenology and climate, but also wind direction. The latter is not a dominant effect, as the NEE in Figure 7a is almost the same as the whole-region average NEE for the same time (Riley et al. 2009). Using the ISOLSM ^{13}C routines and the same upwind sub-regions, we predicted δ_{bio} at the Central Facility tower. These predictions match the observed values for δ_{bio} within 1-2‰ most of the time, both in magnitude and in weekly and seasonal variability, but there were some weeks with larger differences (Figure 7b). Figure 7c shows 2006–2008 isoflux calculated as the product of predicted NEE and predicted δ_{bio}.

Four patterns are evident in the isoflux results. First, the timing and broad seasonal pattern of isoflux mirrors that of observed δ_{bio}, with late-winter and mid-summer extremes. Second, the relative amplitude of variation is much larger for isofluxes than for δ_{bio} due to covariance in δ_{bio} and NEE seasonality. Peak uptake occurs in April and May, when the winter wheat is at peak productivity and growth of C_3 grassland species has begun. In other words, the most negative NEE coincides with relatively negative δ_{bio}, and thus the isoflux also peaks in this period.

Third, inter-annual variability in predicted isoflux was large and the dominant cause was variation in NEE rather than in δ_{bio} (Figure 7a and 7b). Specifically, 2006 had much lower peak and cumulative isoflux than did 2007 or 2008. The cumulative annual isoflux upwind of the tower was 0.6, 1.4, and 1.8 MgC ‰ m^{-2} y^{-1} in 2006, 2007, and 2008 respectively. Similarly, 2008 had the largest summertime isoflux of the three years, even though it had almost the same δ_{bio} as in 2007, highlighting the importance of the inter-annual variability in NEE. Finally, in all three years, cumulative modeled NEE was negative (a net carbon sink) leading to a positive isoflux. In other words, because the land surface in this region is predicted to be a net carbon sink (due at least in part to export of agricultural products out of the region, and therefore not being returned to the soil), the annual isoflux caused a net enrichment of δ_{atm} in this region.

4 Discussion

4.1 Seasonal and inter-annual patterns in δ_{atm} and δ_{bio}

While atmospheric δ_{atm} values in SGP followed the global seasonal and annual patterns for this latitude, the δ_{bio} in SGP had much larger seasonality and was strongly influenced by local land use and land cover change. The measured weekly δ_{bio} varied by 8‰ seasonally, from spring minimum to summer maximum, with little interannual variation in this cycle across the 8-year record.

Keeling plot intercepts generated by nighttime and daylight sampling are affected by different processes. The nighttime intercept captures only ecosystem respiration, and may reflect small changes in footprint throughout the night. The diel intercept is influenced by a growing boundary layer, isotopic composition of both photosynthesis and heterotrophic respiration, and changing footprints (Pataki et al. 2003; Griffis et al. 2007; Shimoda et al. 2009). Nevertheless, when comparing light and dark plots from the same week, or diel and nighttime plots from consecutive weeks, we observed similar δ_{bio} values (Figure 6; Figure 5). Although the larger range of CO_2 values and unidirectionality of nighttime CO_2 fluxes tended to yield lower SE values, about one third of the day time samplings at SGP resulted in good Keeling plot intercepts.

We can explore potential isotopic disequilibrium between photosynthesis and respiration by comparing the diel-light and diel-dark Keeling intercepts from the same 24-h diel sampling. The diel-dark values were slightly more negative on average (-0.49 ±0.27‰, n=30) than the

paired diel-light values. As noted above, the difference could be due to isotopic disequilibrium as well as atmospheric mixing and transport. The fact that half of the light-dark comparisons, distributed in spring, summer, and fall, showed no difference (-0.03 ±0.25‰, n=16 of 30) suggests there was no difference between the respiratory and NEE δ_{bio} values during those times; the alternative hypothesis is that a complex coincidence of atmospheric conditions and land-surface exchanges compensated for a real difference. In any case, the day-night differences in any given diurnal cycle were much lower than the seasonal variations associated with shifts in C_3-C_4 fractions.

There are a few properties of SGP that could create large disequilibrium between the isotopic signatures of heterotrophic respiration and net photosynthetic fluxes. First, C_3 and C_4 plants tend to have different phenology, whether growing together in grasslands or in different fields. If ecosystem respiration lags productivity on order of months, there would be significant C_3 carbon respired during peak C_4 productivity, or vice-versa. Second, farmers may plant a C_3 crop in fields that had C_4 plants the previous year, or vice-versa. We could deduce disequilibrium between respiration and photosynthesis if we observed differences in δ_{bio} between the light and dark segments of each diel sampling or from a relatively positive δ_{bio} in months when there was no active C_4 growth, i.e., October–April. Since we did not observe a large day-night difference, and did not see more than 15% C_4 fraction in the winter, our observations suggest that in this region most respiration is of recently photosynthesized material.

4.2 Fractional contribution of C_3 and C_4 plant types to ecosystem carbon exchange

Using a two-member mixing model with leaf-$\delta^{13}C$ end members for C_3 and C_4 vegetation (Table 1), we estimated that ecosystem respiration and NEE in the study region varied from 80% C_3 in winter-spring to 50% C_3 in summer-fall (Table 2). The spring shift from C_3 dominance to balanced C_3-C_4 carbon exchange coincided with the timing of wheat senescence and harvest. We observed fairly consistent seasonal cycles in the C_3:C_4 ratio of ecosystem carbon fluxes despite large variation in weather conditions and model estimates of regional NEE. There was only a weak positive correlation between anomalies in precipitation and δ_{bio} in the summer months.

The observed seasonal cycle of δ_{bio} was too large to explain by water stress, phenology, or disequilibrium between photosynthesis and respiration alone. Rather, the large seasonal changes reflect changes in the relative contribution of C_3- versus C_4-derived fluxes to the air

sampled at the Central Facility. We cannot say, however, that the observed changes in δ_{bio} reflect a change in C_3 and C_4 exchange from a particular set of fields (i.e., a static footprint). It is possible that the footprint influencing the tower air changes over time in such a way that it samples regions of different C_3 and C_4 activity. Both explanations are plausible at this site. For the static footprint case, previous studies have shown that the phenology of the dominant C_3 and C_4 crops and grasses in the study region follow the δ_{bio} pattern we observed (Fischer et al. 2008; Billesbach et al. 2004; Suyker et al. 2003; Still et al. 2003b). For the second case, the SGP quadrant southeast of the tower has more C_4 productivity compared to southwest of the tower, and the prevailing wind typically shifts slightly from southwest to southeast in late spring, coincident with the observed increase in δ_{bio}. Both phenomena—seasonal shifts in C_3 and C_4 productivity and seasonal shifts in wind direction—may be convolved in the patterns reported here.

Prior studies of nighttime δ_{bio} in prairie and pastures report large seasonal cycles in δ_{bio} due to changing proportions of C_4 and C_3 activity (Still et al. 2003a; Lai et al. 2003, 2006). Our summer results are consistent with the δ_{bio} values and seasonal pattern of previous studies. But the annual cycle we report has important differences, notably a larger seasonal δ_{bio} amplitude, because we observed a larger region that included wheat and other C_3 crops in addition to grasslands. Our sampling footprint was larger than that of these earlier studies, which were conducted using shorter towers (<5 m) and in some cases shorter duration for Keeling plot sampling.

Those prior studies also found that higher-than-average spring precipitation increased the C_3 contribution to spring respiration (Still et al. 2003a) and less spring rainfall corresponded to reduced C_4 contribution to summer ecosystem respiration via impacts of spring soil water on the C_3-to-C_4 transition (Lai et al. 2003, 2006). The positive effect of precipitation on summer δ_{bio} within mixed C_3-C_4 grasslands arises because C_4 grasses can outcompete C_3 vegetation during the warmer months. We saw evidence of a weak, positive precipitation response during July and September. We did not see as strong a precipitation response in C_3:C_4 ratio because multiple fields influenced our observations, including summer C_3 monocultures that are also stimulated by higher rainfall.

One caveat to our use of a two-member mixing model to estimate C_3 and C_4 fractions is that fossil emissions and seasonal burning are sources of CO_2 in SGP. Three winter Keeling plot-intercepts gave δ_{bio} less than -30‰, indicating that there was a source of very depleted CO_2, such as fossil fuel-derived CO_2, that was observable when plant and soil fluxes were very small—and thus should be included as a third end member in the mixing model. However, for most of the year ecosystem fluxes are much larger than fossil CO_2 emissions, and therefore likely to have a much greater influence on atmospheric CO_2 concentrations and δ_{atm}.

4.3 Historic δ_{bio}

The observed pattern of C_3-dominated fluxes is very different from that of the native vegetation in this region. We have measured the $\delta^{13}C$ of soil organic carbon (SOC) in native prairie and pasture as well as in fields that were converted from prairie to winter wheat many years ago. The native prairie soil at GRL had $\delta^{13}C$ values of -14.9‰ (SE=0.2, n=48). This indicates a historical ecosystem with about 85% C_4 net primary productivity. In contrast, the surface soil carbon under a field at the Central Facility that had been cultivated with winter wheat for at least the prior decade had $\delta^{13}C$ values around -22‰ in 2004. Thus, as a result of land cover conversion, both the phenology of plant uptake and its isotopic signature have changed significantly in the Southern Great Plains. In addition, during the period when C_4-derived SOC was being replaced with C_3–derived SOC under long-term wheat cultivation, the region must have been a source of ^{13}C to the atmosphere, because soil carbon in the vast prairie areas converted to C_3 crops was becoming lighter, perhaps 7-12‰ lighter.

Observations of δ_{bio} are useful for inverse models that utilize δ_{atm} measurements as a constraint (e.g., Rayner et al. 2008). For example, parameterizing the region with the historic vegetation would result in large errors in estimated δ_{bio}. Likewise, assuming a constant year-round δ_{bio} value, be it C_4 or C_3, would create large errors. For inversions and other purposes, such agricultural regions cannot be simply categorized as C_3 or C_4, or represented by historical vegetation type (Lai et al. 2003; Shimodo et al. 2009).

4.4 Isotopic Disequilibria

While SGP does not appear to have a large ^{13}C disequilibrium on diurnal timescales, it has very large seasonal variation, with a $\delta^{13}C$ amplitude of ~8‰. This variation is due mainly to

the seasonal transition from C_3 to C_4 photosynthesis, and the fact that most respired CO_2 was from recently photosynthesized carbon. On annual timescales, we see a net transfer of ^{13}C between atmosphere and ecosystem because the landscape is a net carbon sink, primarily due to the export of NPP in plant and animal products. Finally, historically this region shows a decadal to centennial disequilibrium due to historical land cover change from C_4 to C_3. The large decrease in δ_{bio} due to land cover change increases the ^{13}C signal between ocean uptake and land uptake in this region.

4.5 Isofluxes

The impact of δ_{bio} on atmospheric $^{13}C/^{12}C$ composition depends on the flux rate and the flux $\delta^{13}C$ values. As a result of the covariance in seasonal cycles in δ_{bio} and predicted NEE and, the seasonal amplitude in isoflux was larger proportionally than variation in δ_{bio} (Figure 7). In addition, there was substantial inter-annual variability in isoflux between 2006 and 2008. The seasonal cycle in δ_{bio} did not vary appreciably from year to year. Rather, interannual variability in isoflux in this region mainly results from interannual variability in NEE, which is sensitive to rainfall, other climate conditions, and land use.

Because the land surface in this region is typically a net carbon sink, the annual isoflux causes a net enrichment of atmospheric $^{13}CO_2$ in this region. However, this effect is diminished by the significant contribution to NEE by C_4 plants in this region. For example, the isotopic enrichment in the boundary layer would be roughly 0.016‰ less for each ppm of CO_2 drawdown in mid-summer than it would be if the ecosystem was populated by only C_3 vegetation. This difference may seem small, but given the large CO_2 draw-downs that occur over the mid-continent in summer (Desai et al. 2005), the resulting downwind isotopic signal would be clearly measurable by current technology, and such measurements could assist in identifying the source of the observed CO_2 signal. This difference is also critical for understanding the cumulative change in the concentration and isotopic compostion of CO_2 in the atmosphere over annual and interannual time frames.

4.6 Research Needed: Footprints

Interpretation of δ_{bio} values is limited because there is no published theory for estimating the precise footprint of tower-based observations of δ_{bio}. Some of the change in $\delta^{13}C$ between flasks in a single collection period may come from changes in background air advection (i.e., footprint) rather than in ecosystem fluxes. While there are fairly established protocols for estimating the footprint influence function for atmospheric concentration measurements and for fluxes estimated from high frequency observations by eddy covariance analysis, it is more difficult to determine the footprint for a Keeling plot intercept. The measurements in the Keeling plot regression may each have a different footprint because they were collected at different heights and/or times (Griffis et al. 2007). Studies using low towers (< 5 m above the ground) have assumed that the footprint is field scale (100's of m) (Pataki et al. 2003; Still et al. 2003a), but the use of different sampling heights can complicate interpretation even over low-statured vegetation (Pataki et al. 2003). Analyses of $\delta^{13}C$ data from tall towers, like WLEF in Park Falls, Wisconsin, have assumed a large, regional footprint, but to our knowledge these footprints have not been quantified. In one comparison, the estimated footprint for Keeling plots (based on the individual concentration footprints) was up to 20 times greater than the footprint of the co-located eddy covariance measurements (Griffis et al. 2007). More footprint quantification tools are needed to take advantage of opportunities for combining CO_2 eddy flux measurements with Keeling plot or ^{13}C eddy flux results.

4.7 Summary and Implications

We report here one of the longest time series available of the $\delta^{13}CO_2$ value (δ_{bio}) of ecosystem carbon fluxes. The data are available from the ARM archive (www.arm.gov) or the authors. In the heterogeneous, agricultural Southern Great Plains, there was a consistent seasonal cycle in δ_{bio}, with large amplitude of almost 8‰ due to C_3 dominance in spring and C_4 dominance in summer. Because of land cover change to C_3 crops, the regional isotopic signature of plant uptake in SGP is currently much more negative (roughly -20 to -27‰) compared to historic soil carbon values (roughly -15‰). Although the seasonal cycle in δ_{bio} was fairly constant from year to year, there were large seasonal and inter-annual variations in predicted isoflux, due to seasonal covariance of NEE and δ_{bio} and inter-annual variation in NEE.

Carbon sources and sinks inferred by atmospheric carbon budgets can depend strongly on the assumed $\delta^{13}C$ value of ecosystem CO_2 exchanges (Ciais et al. 1995, 1999; Fung et al. 1997; Scholze et al. 2008). For the Southern Great Plains, assuming historic or potential vegetation would result in large errors in estimated δ_{bio} and thus in regional to global carbon flux estimates. Likewise, assuming a constant $\delta^{13}C$ value of NEE year-round could create large errors in inferred fluxes. As a result, grasslands and savannah, as well as agricultural regions should not be categorized as purely C_3 or C_4, or represented by historical vegetation types, because land use and land cover change on seasonal to decadal timescales can have large impacts on the isotopic fluxes between the land surface and atmosphere.

Acknowledgments

We thank Larry Giles, Marc Fischer, Cristina Castanha, and Deb Williard for assistance with sampling and sample analysis, USDA Grazinglands Research Laboratory for site access, and NOAA ESRL for atmospheric network observations, the GLOBALVIEW product, and calibration standards. This research was supported by the Office of Biological and Environmental Research of the U.S. Department of Energy under Contract No. DE-AC02-05CH11231 as part of the Atmospheric Radiation Measurement Program.

References

Ackerman, T.P., Genio A.D.D., Ellingson R.G., Ferrare R.A., Klein S.A., McFarquhar G.M., Lamb P.J., Long C.N., and Verlinde J. 2004. Atmospheric Radiation Measurement Program Science Plan: Current Status and Future Directions of the ARM Science Program, U. S. Department of Energy, Office of Biological and Environmental Research., edited.

Aranibar, J.N., Berry J.A., Riley W.J., Pataki D.E., Law B.E., and Ehleringer J.R. 2006. Combining meteorology, eddy fluxes, isotope measurements, and modeling to understand environmental controls of carbon isotope discrimination at the canopy scale. *Global Change Biology* **12**, 710-730.

Bakwin, P.S., Tans P.P., White J.W.C., and Andres R.J. 1998. Determination of the isotopic ($^{13}C/^{12}C$) discrimination by terrestrial biology from a global network of observations. *Global Biogeochemical cycles* **12**, 555-562.

Battle, M., Bender M.L., Tans P.P., White J.W.C., Ellis J.T., Conway T., and Francey R.J. 2000. Global carbon sinks and their variability inferred from atmospheric O_2 and $d^{13}C$. *Science* **287**, 2467-2470.

Billesbach, D.P., Fischer M.L., Torn M.S., and Berry J.A. 2004. A portable eddy covariance system for the measurement of ecosystem-atmosphere exchange of CO_2, water vapor, and energy. *Journal of Atmospheric and Oceanic Technology* **21**, 639-650.

Bowling, D.R., Baldocchi D.D., and Monson R.K. 1999. Dynamics of isotopic exchange of carbon dioxide in a Tennessee deciduous forest. *Global Biogeochemical Cycles* **13**, 903-922.

Bowling, D.R., Pataki D.E., and Randerson J.T. 2008. Carbon isotopes in terrestrial ecosystem pools and CO_2 fluxes. *New Phytologist* **178**, 24-40.

Buchmann, N., Brooks J.R., Rapp K.D., and Ehleringer J.R. 1996. Carbon isotope composition of C_4 grasses is influenced by light and water supply. *Plant Cell and Environment* **19**, 392-402.

Buchmann, N., and Ehleringer J.R. 1998. CO_2 concentration profiles, and carbon and oxygen isotopes in C_3 and C_4 crop canopies. *Agricultural and Forest Meteorology* **89**, 45-58.

Cernusak, L.A., Tcherkez G., Keitel C., Cornwell W.K., Santiago L.S., Knohl A., Barbour M.M., Williams D.G., Reich P.B., Ellsworth D.S., Dawson T.E., Griffiths H.G., Farquhar G.D., and Wright I.J. 2009. Viewpoint: Why are non-photosynthetic tissues generally C-13 enriched compared with leaves in C-3 plants? Review and synthesis of current hypotheses. *Funct. Plant Biol.* **36**, 199-213.

Ciais, P., Tans P.P., Trolier M., White J.W.C., and Francey R.J. 1995. A large northern-hemisphere terrestrial CO_2 sink indicated by the $^{13}C/^{12}C$ ratio of atmospheric CO_2. *Science* **269**, 1098-1102.

Ciais, P., Friedlingstein P., Schimel D.S., and Tans P.P. 1999. A global calculation of the $d^{13}C$ of soil respired carbon: Implications for the biospheric uptake of anthropogenic CO_2. *Global Biogeochemical Cycles* **13**, 519-530.

Collatz, G.J., Berry J.A., and Clark J.S. 1998. Effects of climate and atmospheric CO_2 partial pressure on the global distribution of C_4 grasses: present, past, and future. *Oecologia* **114**, 441-454.

Dawson, T.E., Mambelli S., Plamboeck A.H., Templer P.H., and Tu K.P. 2002. Stable isotopes in plant ecology. *Annual Review of Ecology and Systematics* **33**, 507-559.

Desai, A.R., Noormets A., Bolstad P.V., Chen J.Q., Cook B.D., Davis K.J., Euskirchen E.S., Gough C.M., Martin J.G., Ricciuto D.M., Schmid H.P., Tang J.W., and Wang W.G. 2008. Influence of vegetation and seasonal forcing on carbon dioxide fluxes across the Upper Midwest, USA: Implications for regional scaling. *Agricultural and Forest Meteorology* **148**, 288-308.

Edwards, E.J., and Still C.J. 2008. Climate, phylogeny and the ecological distribution of C_4 grasses. *Ecology Letters* **11**, 266-276.

Ehleringer, J.R., Cerling T.E., and Helliker B.R. 1997. C_4 photosynthesis, atmospheric CO_2 and climate. *Oecologia* **112**, 285-299.

Enting, I.G., Trudinger C.M., and Francey R.J. 1995. A synthesis inversion of the concentration and $d^{13}C$ of atmospheric CO_2. *Tellus* **47B**, 35-52.

Epstein, H.E., Lauenroth W.K., Burke I.C., and Coffin D.P. 1997. Productivity patterns of C_3 and C_4 functional types in the US Great Plains. *Ecology* **78**, 722-731.

Farquhar, G.D., Ehleringer J.R., and Hubick K.T. 1989. Carbon isotope discrimination and photosynthesis. *Annual Review of Plant Physiology and Plant Molecular Biology* **40**, 503-537.

Fischer, M.L., Billesbach D.P., Berry J.A., Riley W.J., and Torn M.S. 2008. Spatiotemporal variations in growing season exchanges of CO_2, H_2O, and sensible heat in agricultural fields of the Southern Great Plains. *Earth Interactions* **11**.

Flanagan, L.B., Brooks J.R., Varney G.T., Berry S.C., and Ehleringer J.R. 1996. Carbon isotope discrimination during photosynthesis and the isotope ratio of respired CO_2 in boreal forest ecosystems. *Global Biogeochemical Cycles* **10**, 629-640.

Flanagan, L.B., and Ehleringer A.R. 1998. Ecosystem-atmosphere CO_2 exchange: interpreting signals of change using stable isotope ratios. *Trends in Ecology & Evolution* **13**, 10-14.

Francey, R.J., Tans P.P., Allison C.E., Enting I.G., White J.W.C., and Trolier M. 1995. Changes in oceanic and terrestrial carbon uptake since 1982. *Nature* **373**, 326-330.

Freeman, C.C. 1998. The Flora of Konza Prairie: A Historical Review and Contemporary Patterns, in *Grassland Dynamics*. edited by A. K. Knapp, Briggs, J. M., Hartnett, D. C., Collins, S. L., pp. 69-80, New York, Oxford University Press.

Friedli, H., Siegenthaler U., Rauber D., and Oeschger H. 1987. Measurements of concentration, $^{13}C/^{12}C$ and $^{18}O/^{16}O$ ratios of tropospheric carbon dioxide over Switzerland. *Tellus* **39B**, 80-88.

Fung, I., Field C.B., Berry J.A., Thompson M.V., Randerson J.T., Malmstrom C.M., Vitousek P.M., Collatz G.J., Sellers P.J., Randall D.A., Denning A.S., Badeck F., and John J. 1997. Carbon 13 exchanges between the atmosphere and biosphere. *Global Biogeochemical Cycles* **11**, 507-533.

Griffis, T.J., Zhang J., Baker J.M., Kljun N., and Billmark K. 2007. Determining carbon isotope signatures from micrometeorological measurements: Implications for studying biosphere-atmosphere exchange processes. *Boundary-layer Meteorology* **123**, 295-316.

Harwood, K.G., Gillon J.S., Roberts A., and Griffiths H. 1999. Determinants of isotopic coupling of CO_2 and water vapour within a Quercus petraea forest canopy. *Oecologia* **119**, 109-119.

Heimann, M., and Maier-Reimer E. 1996. On the relations between the oceanic uptake of CO_2 and its carbon isotopes. *Global Biogeochemical Cycles* **10**, 89-111.

Henderson, S.A., Voncaemmerer S., and Farquhar G.D. 1992. Short-term measurements of carbon isotope discrimination in several C_4 species. *Australian Journal of Plant Physiology* **19**, 263-285.

Keeling, C.D. 1958. The concentration and isotopic abundances of atmospheric carbon dioxide in Rural Areas. *Geochimica Et Cosmochimica Acta* **13**, 322-334.

Keeling, C.D. 1961. The concentration and isotopic abundances of carbon dioxide in rural and marine air. *Geochimica Et Cosmochimica Acta* **24**, 277-298.

Keeling, C.D., Bacastow R.B., Carter A.F., Piper S.C., Whorf T.P., Heimann M., Mook W.G., and Roeloffzen H.A. 1989. A three-dimensional model of atmospheric CO_2 transport based on observed winds, 1, Analysis of observational data, in *Aspects of Climate Variability in the Pacific and Western Americas, Geophysical Monogr. Ser.* edited by D. H. Peterson, pp. 165-236, Washington, D.C., AGU.

Keeling, C.D., Whorf T.P., Wahlen M., and van der Plicht J. 1995. Interannual extremes in the rate of rise of atmospheric carbon dioxide since 1980. *Nature* **375**, 666-670.

Kemp, P.R., and Williams G.J. 1980. A physiological-basis for niche separation between Agropyron-smithii (C_3) and Bouteloua-gracilis (C_4). *Ecology* **61**, 846-858.

Knapp, A.K., Briggs J.M., and Turner C.L. 1998. Patterns and controls of aboveground net primary production in tallgrass prairie, in *Grassland dynamics*. edited by A. K. Knapp, Briggs, J. M., Hartnett, D. C., Collins, S. L., pp. 193-221, New York, Oxford University Press.

Lai, C.T., Schauer A.J., Owensby C., Ham J.M., and Ehleringer J.R. 2003. Isotopic air sampling in a tallgrass prairie to partition net ecosystem CO_2 exchange. *Journal of Geophysical Research-Atmospheres* **108**, 4566.

Lai, C.T., Schauer A.J., Owensby C., Ham J.M., Helliker B., Tans P.P., and Ehleringer J.R. 2006. Regional CO_2 fluxes inferred from mixing ratio measurements: estimates from flask air samples in central Kansas, USA. *Tellus* **58B**, 523-536.

Langenfelds, R.L., Francey R.J., Pak B.C., Steele L.P., Lloyd J., Trudinger C.M., and Allison C.E. 2002. Interannual growth rate variations of atmospheric CO_2 and its $d^{13}C$, H_2, CH_4, and CO between 1992 and 1999 linked to biomass burning. *Global Biogeochemical Cycles* **16**, 1048.

Laws, E.A. 1997. *Mathematical Methods for Oceanographers: An Introduction*, New York, Wiley & Sons, Inc.

Le Quere, C., Aumont O., Bopp L., Bousquet P., Ciais P., Francey R., Heimann M., Keeling C.D., Keeling R.F., Kheshgi H., Peylin P., Piper S.C., Prentice I.C., and Rayner P.J. 2003. Two decades of ocean CO_2 sink and variability. *Tellus* **55B**, 649-656.

Masarie, K.A., and Tans P.P. 1995. Extension and integration of atmospheric carbon-dioxide data into a globally consistent measurement record. *Journal of Geophysical Research-Atmospheres* **100**, 11593-11610.

McNab, W.H., and Avers P.E. 1994. Ecological Subregions of the United States: Section Descriptions, USDA, Forest Service, Eco- system Management, Washington, D.C.

Miranda, A.C., Miranda H.S., Lloyd J., Grace J., Francey R.J., McIntyre J.A., Meir P., Riggan P., Lockwood R., and Brass J. 1997. Fluxes of carbon, water and energy over Brazilian cerrado: An analysis using eddy covariance and stable isotopes. *Plant Cell and Environment* **20**, 315-328.

Mole, S., Joern A., Oleary M.H., and Madhavan S. 1994. Spatial and temporal variation in carbon-isotope discrimination in prairie graminoids. *Oecologia* **97**, 316-321.

Niu, S.L., Liu W.X., and Wan S.Q. 2008. Different growth responses of C_3 and C_4 grasses to seasonal water and nitrogen regimes and competition in a pot experiment. *Journal of Experimental Botany* **59**, 1431-1439.

Pataki, D.E., Ehleringer J.R., Flanagan L.B., Yakir D., Bowling D.R., Still C.J., Buchmann N., Kaplan J.O., and Berry J.A. 2003. The application and interpretation of Keeling plots in terrestrial carbon cycle research. *Global Biogeochemical Cycles* **17**, 22-35.

Phillips, D.L., and Gregg J.W. 2001. Uncertainty in source partitioning using stable isotopes. *Oecologia* **127**, 171-179.

Randerson, J.T., Thompson M.V., and Field C.B. 1999. Linking ^{13}C-based estimates of land and ocean sinks with predictions of carbon storage from CO_2 fertilization of plant growth. *Tellus* **51B**, 668-678.

Randerson, J.T., Still C.J., Balle J.J., Fung I.Y., Doney S.C., Tans P.P., Conway T.J., White J.W.C., Vaughn B., Suits N., and Denning A.S. 2002. Carbon isotope discrimination of arctic and boreal biomes inferred from remote atmospheric measurements and a biosphere-atmosphere model. *Global Biogeochemical cycles* **16**, 1136.

Randerson, J.T., van der Werf G.R., Collatz G.J., Giglio L., Still C.J., Kasibhatla P., Miller J.B., White J.W.C., DeFries R.S., and Kasischke E.S. 2005. Fire emissions from C_3 and C_4 vegetation and their influence on interannual variability of atmospheric CO_2 and $d^{13}CO_2$. *Global Biogeochemical Cycles* **19**, GB2019.

Rayner, P.J., Enting I.G., Francey R.J., and Langenfelds R. 1999. Reconstructing the recent carbon cycle from atmospheric CO_2, $d^{13}C$ and O_2/N_2 observations. *Tellus* **51B**, 213-232.

Rayner, P.J., Law R.M., Allison C.E., Francey R.J., Trudinger C.M., and Pickett-Heaps C. 2008. Interannual variability of the global carbon cycle (1992-2005) inferred by inversion of atmospheric CO_2 and $d^{13}CO_2$ measurements. *Global Biogeochemical Cycles* **22**, GB3008.

Ribas-Carbo, M., Still C., and Berry J. 2002. Automated system for simultaneous analysis of $d^{13}C$, $d^{18}O$ and CO_2 concentrations in small air samples. *Rapid Communications in Mass Spectrometry* **16**, 339-345.

Riley, W.J., Still C.J., Helliker B.R., Ribas-Carbo M., and Berry J.A. 2003. ^{18}O composition of CO_2 and H_2O ecosystem pools and fluxes in a tallgrass prairie: Simulations and comparisons to measurements. *Global Change Biology* **9**, 1567-1581.

Riley, W.J., Biraud S.C., Torn M.S., Fischer M.L., Billesbach D.P., and Berry J.A. 2009. Regional CO_2 and latent heat surface fluxes in the Southern Great Plains: Measurements, modeling, and scaling. *Journal Of Geophysical Research-Biogeosciences* **114**, G04009.

Scholze, M., Ciais P., and Heimann M. 2008. Modeling terrestrial ^{13}C cycling: Climate, land use and fire. *Global Biogeochemical Cycles* **22**, B1009.

Shimoda, S., Murayama S., Mo W., and Oikawa T. 2009. Seasonal contribution of C_3 and C_4 species to ecosystem respiration and photosynthesis estimated from isotopic measurements of atmospheric CO_2 at a grassland in Japan. *Agricultural and Forest Meteorology* **149**, 603-613.

Sokal, R.R., and Rohlf F.J. 1995. *The Principles and Practice of Statistics in Biological Research*. 3rd ed., New York, W. H. Freeman.

Still, C.J., Berry J.A., Collatz G.J., and DeFries R.S. 2003a. Global distribution of C_3 and C_4 vegetation: Carbon cycle implications. *Global Biogeochemical Cycles* **17**, 1006.

Still, C.J., Berry J.A., Ribas-Carbo M., and Helliker B.R. 2003b. The contribution of C_3 and C_4 plants to the carbon cycle of a tallgrass prairie: an isotopic approach. *Oecologia* **136**, 347-359.

Suyker, A.E., Verma S.B., and Burba G.G. 2003. Interannual variability in net CO2 exchange of a native tallgrass prairie. *Global Change Biology* **9**, 255-265.

Tans, P.P., Berry J.A., and Keeling R.F. 1993. Oceanic $^{13}C/^{12}C$ observations: A new window on ocean CO_2 uptake. *Global Biogeochemical Cycles* **7**, 353-368.

Tieszen, L.L., Reed B.C., Bliss N.B., Wylie B.K., and DeJong D.D. 1997. NDVI, C_3 and C_4 production, and distributions in great plains grassland land cover classes. *Ecological Applications* **7**, 59-78.

Townsend, A.R., Asner G.P., White J.W.C., and Tans P.P. 2002. Land use effects on atmospheric ^{13}C imply a sizable terrestrial CO_2 sink in tropical latitudes. *Geophysical Research Letters* **29**, 68-71.

Yakir, D., and Sternberg L.D.L. 2000. The use of stable isotopes to study ecosystem gas exchange. *Oecologia* **123**, 297-311.

Zar, J.H. 1996. *Biostatistical Analysis*, Englewood Cliffs, NJ, Prentice Hall.

Zobitz, J.M., Keener J.P., Schnyder H., and Bowling D.R. 2006. Sensitivity analysis and quantification of uncertainty for isotopic mixing relationships in carbon cycle research. *Agricultural and Forest Meteorology* **136**, 56-75.

Tables

Table 1. $\delta^{13}C$ values for green leaves and soil carbon in two grazed tallgrass prairie fields at the USDA Grazinglands Research Laboratory (GRL), El Reno, Oklahoma; and wheat fields and prairie near the ACRF Central Facility, Billings, Oklahoma. For GRL, N = composite of many leaves. For Central Facility wheat, N=1 green leaf and 5 replicate leaves were sampled each month from a single field unless noted. For Still et al. (2003b), N is for number of species sampled, and does not include replicate samples taken through the growing season.

Site	Dates	^{13}C (SE) ‰ C_3 Grasses and Forbs	N	^{13}C (SE) ‰ C_4 Grasses	N	Soil to 1 m	N
Prairie, GRL	May-Dec 2005-2006	-28.56 (0.16)	27	-12.42 (0.23)	18	-14.86 (0.19)	48
Prairie, near Central Facility (Still et al. 2003b)	May-Oct 1999	-28.3‰ (0.8)	12	-12.2‰ (0.7)	4	—	—
Wheat Fields, near Central Facility	Jan-May 2003	-28.04 (0.08)	45	—	—	—	—
Values used as C_3 and C_4 endmembers		-28.2‰		-12.4‰			

Table 2. Ensemble monthly means (each monthly average, averaged for all years) of δ_{bio} for 2002-2009. The uncertainty due to uncertainty in end members, assessed using the standard errors in Table 1, is less than 1.4% for the fractional C_3 and C_4 contributions to ecosystem exchange.

Month	Mean Monthly δ_{bio} (‰)	Std Error of monthly means	N (y)	Fraction C_3 (%)	Fraction C_4 (%)
Jan	-25.3	0.44	5	82	18
Feb	-24.9	0.16	6	79	21
Mar	-25.8	0.43	7	85	15
Apr	-24.9	0.62	7	79	21
May	-23.5	0.37	7	70	30
Jun	-20.8	0.60	7	53	47
Jul	-20.1	0.35	7	49	51
Aug	-20.4	0.23	8	51	49
Sep	-20.4	0.43	7	51	49
Oct	-22.5	0.35	8	64	36
Nov	-23.5	0.49	8	70	30
Dec	-24.8	0.75	5	78	22

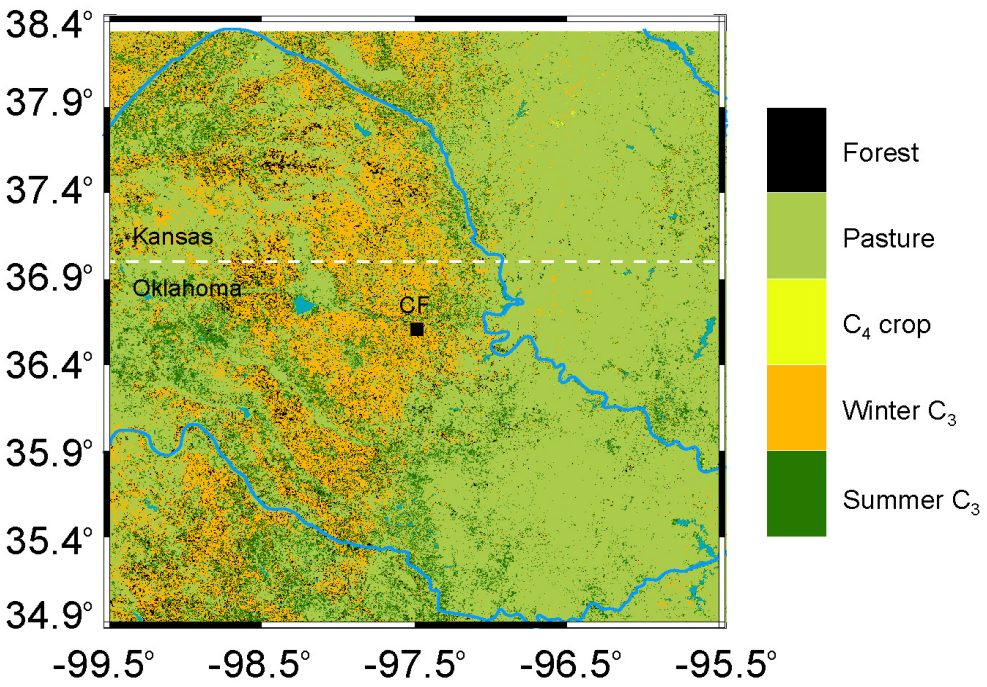

Figure 1. Map of the U.S. Southern Great Plains study region, showing the location of the Central Facility (square), and the distribution of land cover types at 250 m resolution. Land cover is derived from MODIS NDVI retrievals and archetypal phenology (Riley et al., 2009). The boundaries of the map are those of the ARM Climate Research Facility.

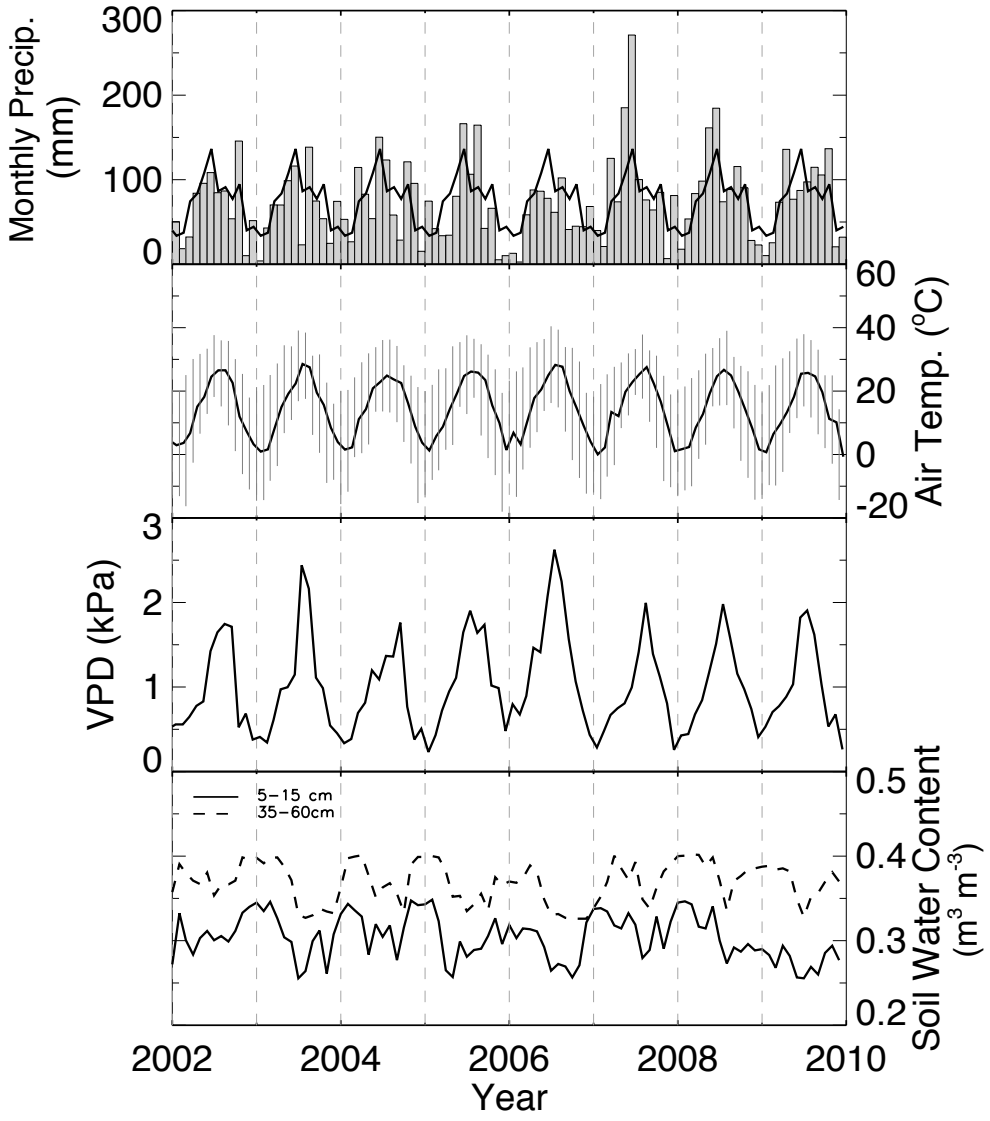

Figure 2. Climate in the Southern Great Plains. (a) Monthly precipitation (bars) and 1996-2008 mean monthly precipitation (line). Temperature, precipitation, and relative humidity (used to calculated vapor pressure deficit) data are interpolated from Oklahoma and Kansas Mesonet stations and averaged for SGP (Riley et al., 2009). (b) Monthly temperature (circles) and 2000-2008 mean monthly temperature (line). (c) vapor pressure deficit (VDP). (d) Soil moisture at 5-35 cm (average of probes at 5, 25, and 35 cm) and 35-60 cm (average of probes at 35 and 60 cm) from ARM SWATS (Soil Water and Temperature System) data.

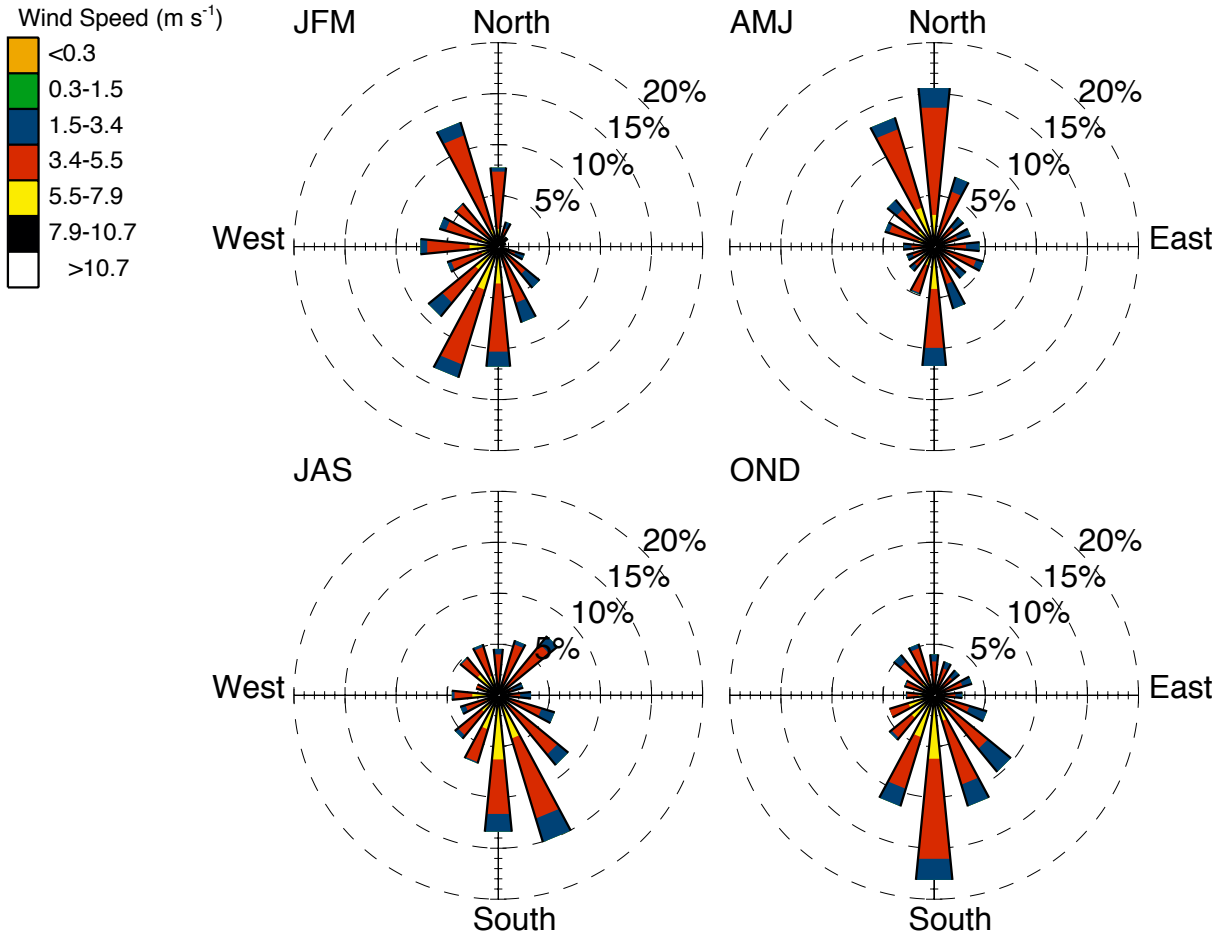

Figure 3. Wind rose for winter, spring, summer, and fall. Based on data collected 4 m above the ground at the ARM Climate Research Facility.

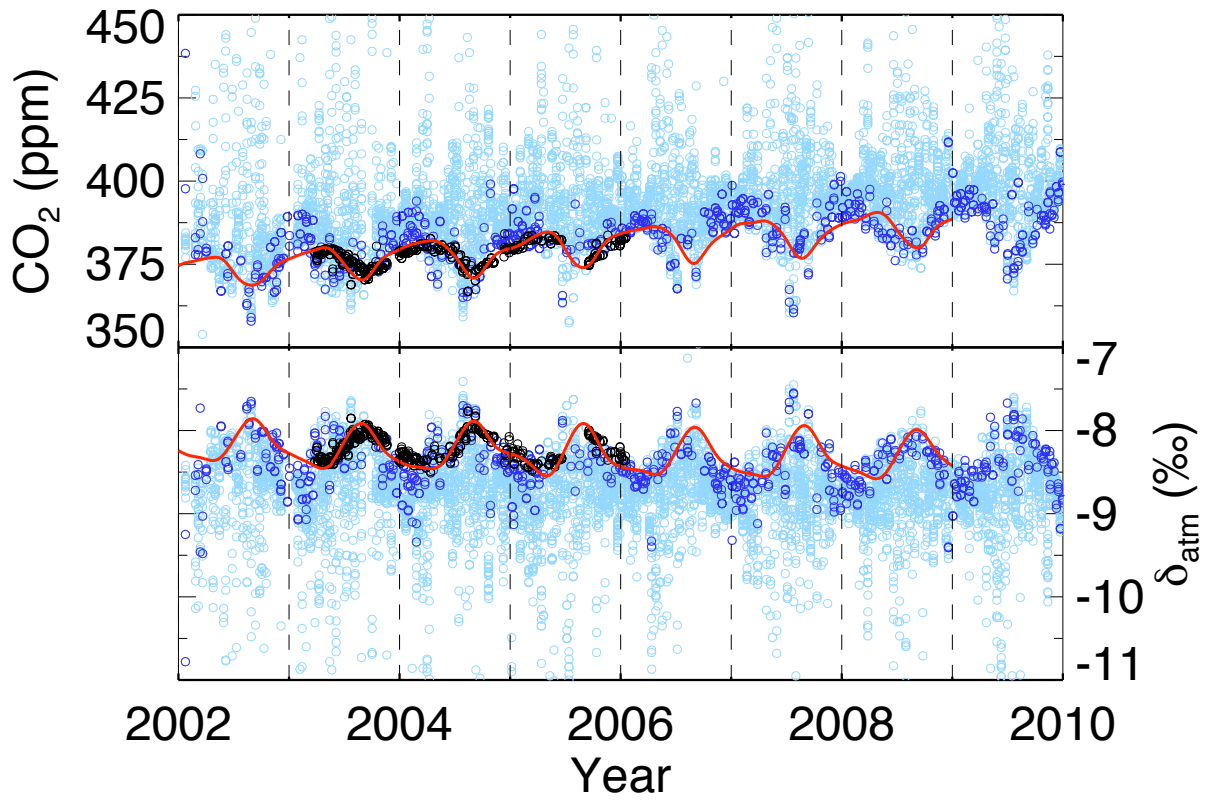

Figure 4. Atmospheric CO_2 mixing ratio (upper panel) and ^{13}C value (δ_{atm}, lower panel) for the global background, free troposphere of SGP, and boundary layer of SGP. In both plots, the red line is the NOAA GLOBALVIEW value for the latitudinal band of the site (http://www.esrl.noaa.gov/gmd/ccgg/globalview/). Black circles are from flasks we collected by aircraft quasi-weekly above the boundary layer (> 3000 m above sea level), which are analyzed by NOAA. The blue circles show the data used in Keeling plots. The dark blue circles are for flasks collected at 2–60 m between 2–5 pm (i.e., in the well mixed boundary layer). The light blue symbols are the flasks collected at 2–60 m at all other times.

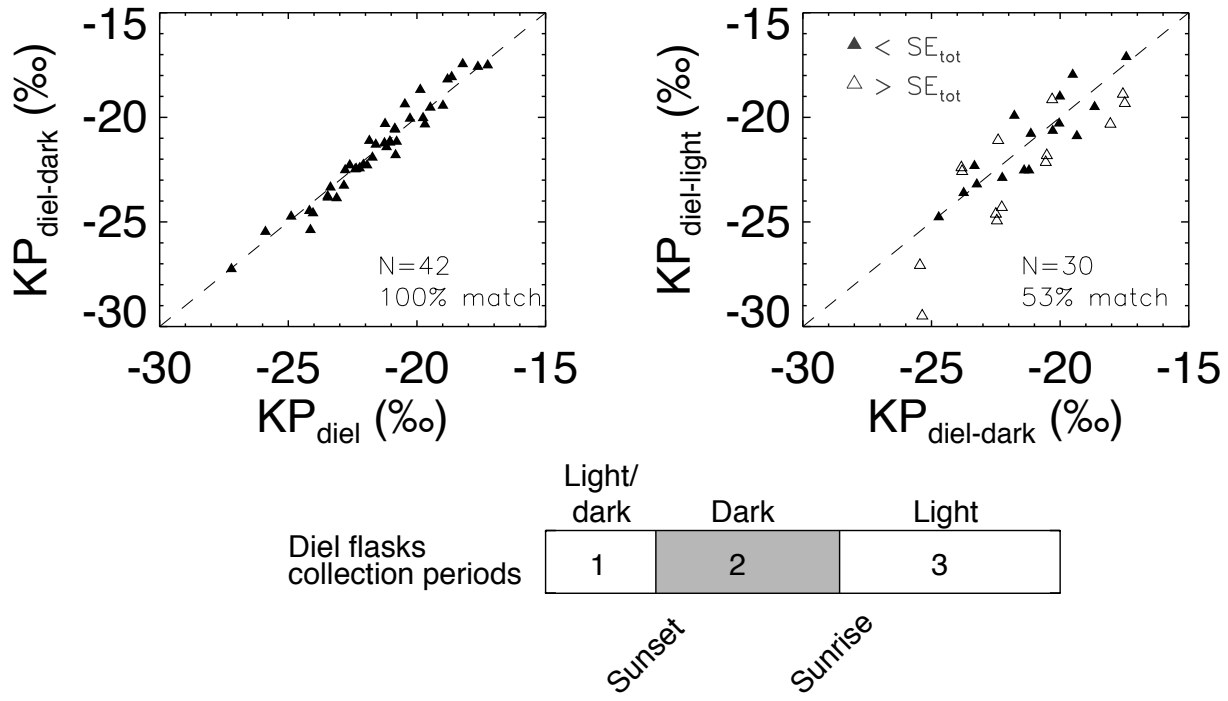

Figure 5. The 21 h diel sampling can be divided into three periods: (1) the late afternoon of the first day, (2) the dark period between sunset and sunrise, and (3) the morning to afternoon of the following day. The left panel compares the Keeling plot intercept generated by the diel-dark flasks (period 2) with that from the whole diel period (period 123). These two δ_{bio} values (i.e., Keeling plot intercepts) matched in 100% of the cases, meaning the difference between the diel and diel-dark-only intercepts was less than the SE of the two values. The right panel shows the relationship between diel-dark and diel-light (period 3) Keeling plot intercepts. The closed symbol indicates that the dark and light values matched; the open symbols indicate a larger difference relative to the SE. In both plots, data are shown only for Keeling plots with SE<1.5‰ (N=42 for dark (2); N=30 for dark and light (3)). The symmetry of scatter around the dashed 1:1 line shows the lack of bias between either the whole diel vs. diel-dark periods or the diel-dark vs. diel-light periods. Flasks were collected every three hours at 2 and 60 m starting at 18:00 local time.

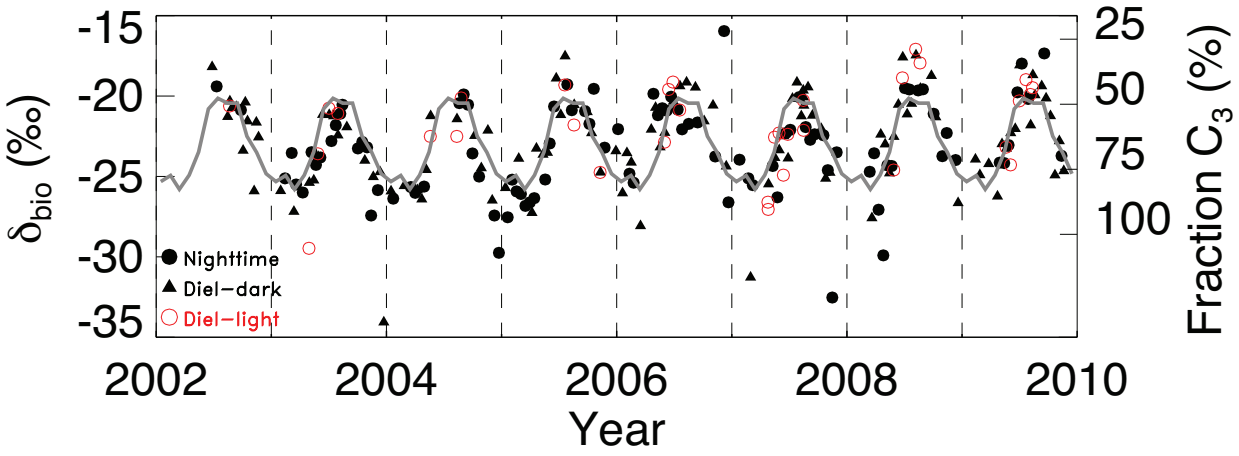

Figure 6. Time series of the isotopic signature of carbon exchange (δ_{bio}) at SGP. Only data with intercept SE < 1.5‰ are shown. The nighttime Keeling plot intercepts (solid circles, n=97) were generated with 16 flasks at four heights overnight. The diel-dark (solid triangles; n = 116) and diel-light (open circle, N = 42) intercepts use flasks from 2 and 60 m collected over a diurnal cycle. There were few day-light Keeling plot intercepts with SE < 1.5‰ between November and February because photosynthetic fluxes and atmospheric $^{13}CO_2$ gradients were too small. The gray line shows the ensemble monthly means for all these data; there were 88 monthly averages for the 96-month period, and the line shows the 8-year ensemble average value for each month (for example, the average of all 8 October's in the record; see Table 2).

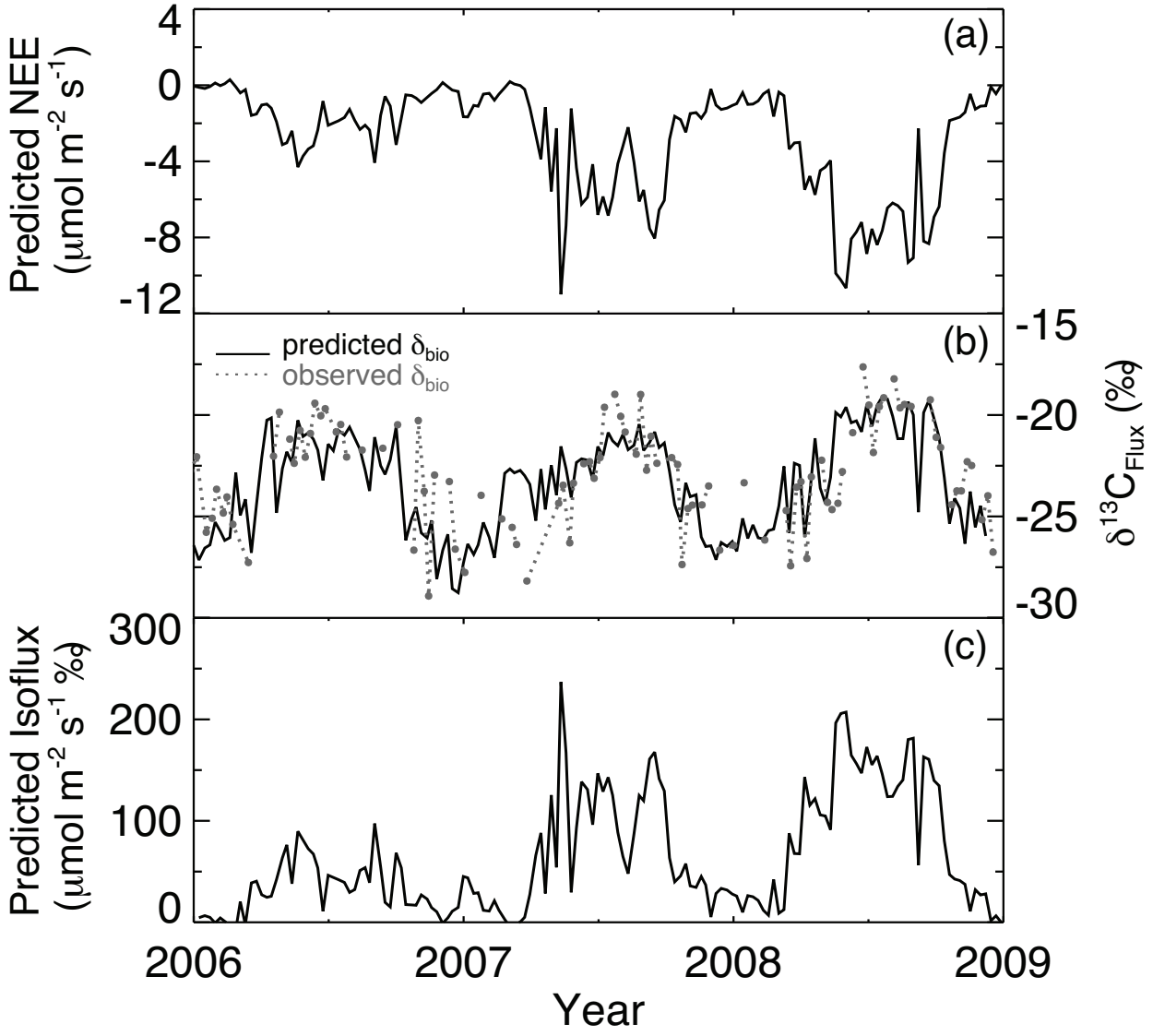

Figure 7. Estimate of isoflux using observed weekly average wind direction, ISOLSM predictions, and Keeling plot results. (a) Average predicted NEE upwind of the observation tower; (b) the δ_{bio} values observed at the tower (dashed line) and predicted by ISOSLM for the SGP quadrant upwind of the observation tower (solid line); and (c) isoflux calculated as NEE × δ_{bio} for each time point using predicted NEE and $\delta_{bio.}$ Positive isoflux means NEE enriches atmospheric δ_{atm}.

Supporting Information Online.

Appendix S1: Figures S1, S2, S3, and S4.

For: Torn, M.S., S. Biraud, C.J. Still, W.J. Riley, J.A. Berry. Seasonal and inter-annual variability in ^{13}C composition of ecosystem carbon fluxes in the U.S. Southern Great Plains. Tellus-B. Accepted September 22, 2010.

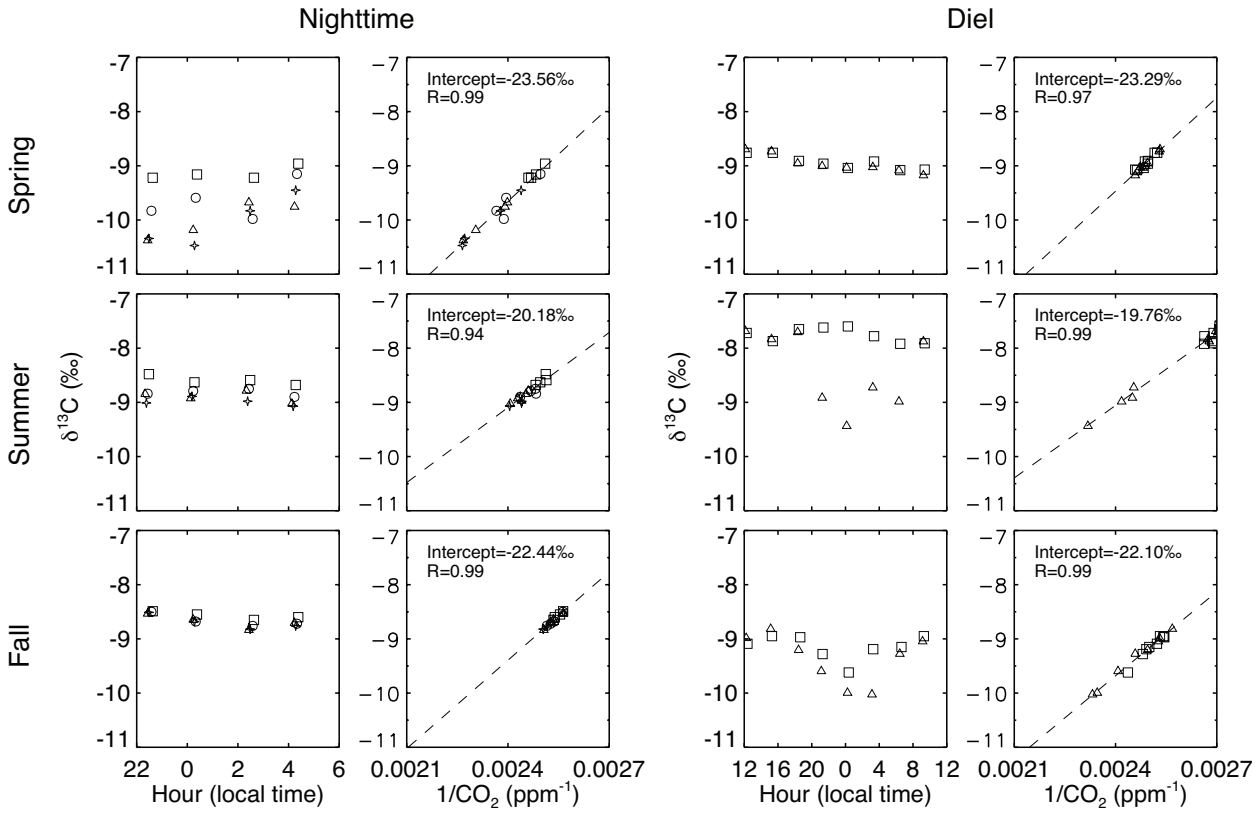

Figure S1. Example of the nighttime and diurnal cycle of $^{13}CO_2$ at different heights above the ground, one week apart, for spring (March 27 and April 2, 2008 for night and diel, respectively), summer (July 29 and July 22, 2009), and fall (October 18 and October 10, 2007). Also shown are the associated Keeling plots intercepts for those data. The symbols indicate flask-collection heights: square = 60 m; circle = 25 m; star = 4 m; triangle = 2 m.

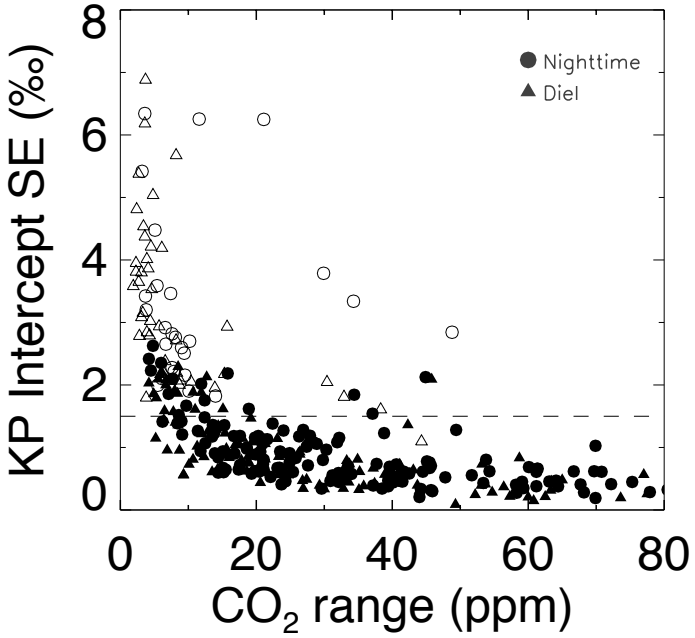

Figure S2. Standard error of the Keeling plot intercept for Nighttime and Diel sampling versus the range of CO2 concentrations for each plot. Solid circles show Keeling plots with linear regression R ≥ 0.9. Open circles are regressions with R < 0.9. The dashed line shows the SE = 1.5‰ threshold employed in this study (n = 234 points below the threshold; n = 97 above). Most intercepts generated from a range of CO2 concentrations > 5 ppm had SE < 1.5‰. The ability to generate significant intercepts with low CO2 ranges was likely due to the large isotopic gradients at our site and high precision of the IRMS used to analyze the samples (Zobitz et al. 2006; Ribas-Carbo et al. 2002).

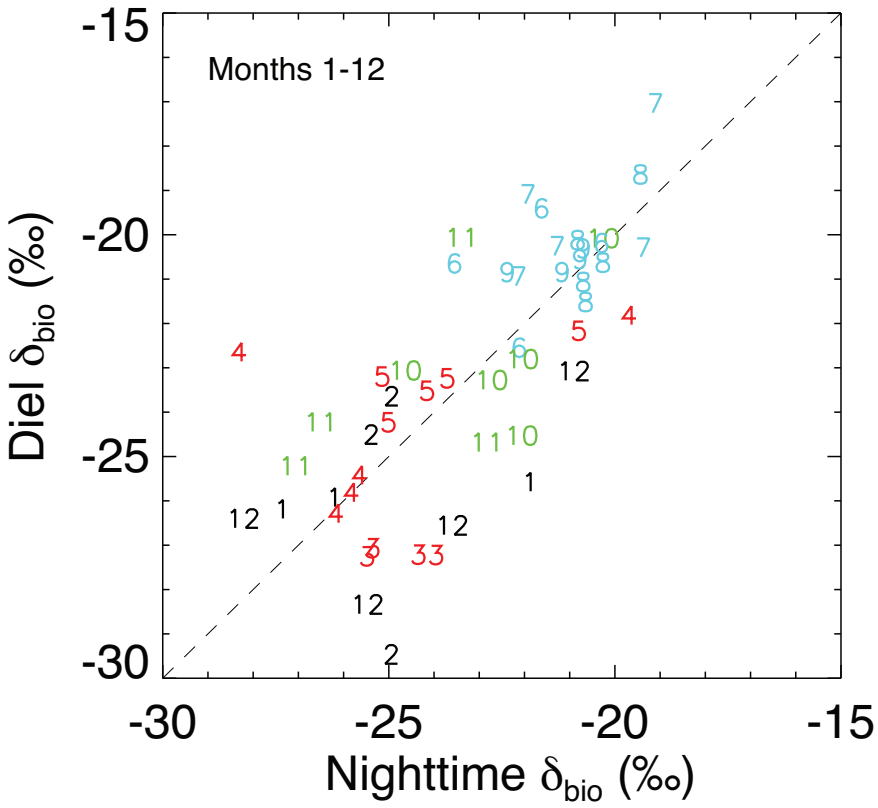

Figure S3. Monthly average Keeling plot intercepts for Nighttime and Diel sampling protocols. Each symbol (number) shows the average value of 1-3 Keeling plots for that month in a given year collected with the Nighttime protocol on the abscissa and with the Diel protocol on the ordinate. The numbers 1-12 indicate months, with colors indicating seasonal periods. The clustering of months (symbol colors) shows seasonal patterns associated with shifts in C_3 and C_4 dominance. Black numbers correspond to the months of December, January, and February (Regression of Nighttime on Diel: R=0.37, N=10, slope =0.32). Red numbers correspond to March, April, and May (R=0.41, N=14, slope =0.39). Blue numbers corresponds to June, July, August, and September (R=0.57, N=18, slope =0.60). Green corresponds to October and November (R=0.55, N=9, slope =0.47).

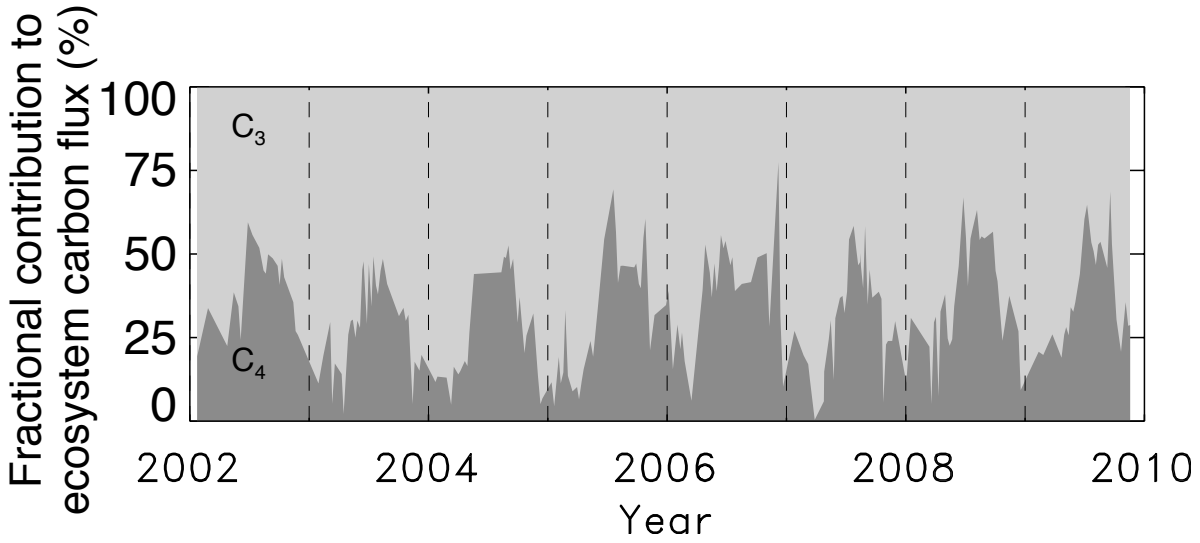

Figure S4. The fractional contribution to total ecosystem respiration from C3 vs. C4 plant types, estimated by a two-member mixing model with end members of -28.2 and -12.4‰, respectively from Still et al., (2003b), this study, and the Nighttime and Diel sampling protocols. The dark and light shading show the C4 and C3 contributions to CO2 flux, respectively. The single dbio value < -30‰ was excluded from this plot.

.